scientific reports

Check for updates

OPEN

Ferromagnetic and half metallic properties of $BaFeO_3$ and $CaFeO_3$ for spintronic applications

K. Bouferrache[1,2], Mohamed A. Habila[3], M. A. Ghebouli[1,4], S. Alomairy[5], Faisal Katib Alanazi[6], M. Fatmi[1]✉ & B. Ghebouli[7]

First-principle calculations were conducted using the Wien2k code with the GGA, mBJ-GGA, and PBE0 (HSE06) functionals. The optimized lattice constants for the cubic unit cells of $CaFeO_3$ and BaFeO3 closely match the experimental values of 3.77 Å and 3.971 Å, respectively. The band structures and densities of states obtained with the mBJ-GGA method, along with the integer magnetic moment of 4 μB per unit cell, confirm the half-metallic nature of $BaFeO_3$ and $CaFeO_3$ in the spin-up channel. Both compounds, characterized by high symmetry, are more stable in the ferromagnetic half-metallic phase. For mBJ-GGA and YS-PBE0(HSE06) functionals, the materials under study are spin-gapless semiconductors. Hybridization of O-2*p* orbital with Fe-3*d* state in the upper valence band for spin-upmakes $BaFeO_3$and $CaFeO_3$as metallic materials. $BaFeO_3$ and $CaFeO_3$ exhibit large absorption coefficient 350×10^4 cm^{-1} and 500×10^4 cm^{-1} in the ultraviolet range, which can be attributed to the infrared phonon mode. The observed refractive index below 1 at the ultraviolet energy is a sign that these materials become superluminal. Furthermore, phonon dispersion calculations revealed the absence of imaginary frequencies across the Brillouin zone, confirming the dynamical stability of both perovskites and reinforcing their suitability for spintronic and optoelectronic applications.

Keywords Perovskites, mBJ-GGA, $BaFeO_3$, $CaFeO_3$, Optoelectronic applications

Alkalines transition metal oxide has specific physical properties, particularly in the transport and magnetic fields. Alkaline earth iron oxide (Ba, Ca)FeO_3 perovskites are interesting materials because theircontrollable ferromagnetic domains. These materials exhibit multiple oxidation states, likely to induce mixed electronic and ionic conductivity. The chemical composition, the nature of cations, as well as the preparation methods influence their physical properties such as electrical conductivity, crystallographic structure, inducing significant modifications of their electrochemical behavior. Calcium-iron oxide is promising for energy storage in so called rechargeable oxide batteries. It possesses favorable properties like good storage capacity for oxygen ions and slow microstructural degradation during repeated reduction and oxidation. Barium iron oxide is highly insoluble, thermally stable, and suitable for glass, optical, and ceramic applications. Inorganic calcium ferrite ($CaFeO_3$) oxide perovskite solar cells material used as hole transport layer provides good stability and high-power conversion efficiency[1]. Thesuper-exchange interactionFe^{+4}–O^{2}–$Fe^{+4}$is responsible for ferromagnetism in $CaFeO_3$ is due to the Fe^{+4}–O^{2}–Fe^{+4}, and its compression to a transition lattice constant causes the loss of its entire magnetic moment and become metallic[2]. The paramagnetic Curie temperature of $CaFeO_3$ is evaluated to be78°K[3]. The bulk modulus of a material can be expressed in terms of the product of ionic charge of their constituents with its lattice parameter[4]. First-principles calculations of the cubic perovskite oxide BaFeO3, performed using density functional theory (DFT) combined with the Hubbard correction (DFT + U) within the generalized gradient approximation, reveal that the material exhibits a half-metallic and ferromagnetic state[5]. The physical properties of both $BaFeO_3$ and $CaFeO_3$ are influenced by their oxygen content, with charge disproportionation occurring through the splitting of Fe^{4+} ions into Fe^{5+} and Fe^{3+} oxidation states[6,7]. A metastable cubic perovskite structure $BaFeO_3$ is considered as a network of [FeO6] octahedra, with linear

[1]Research Unit on Emerging Materials (RUEM), University Ferhat Abbas of Setif 1, Setif 19000, Algeria. [2]Department of Physics, Faculty of Sciences, University of M'sila, University Pole, Road Bourdj Bou Arreiridj, M'sila 28000, Algeria. [3]Department of Chemistry, College of Science, King Saud University, P.O. Box 2455, Riyadh 11451, Saudi Arabia. [4]Department of Chemistry, Faculty of Sciences, University of M'sila, University Pole, Road Bourdj Bou Arreiridj, M'sila 28000, Algeria. [5]Department of Physics, College of Sciences, Taif University, Taif 21944, Saudi Arabia. [6]Department of Physics, College of Sciences, Northern Border University, Arar 73222, Saudi Arabia. [7]Laboratory for the Study of Surfaces and Interfaces of Solid Materials (LESIMS), University Ferhat Abbas of Setif 1, Setif 19000, Algeria. ✉email: fatmimessaoud@yahoo.fr

Fe–O–Fe arrangements[8]. The structure of $BaFeO_3$ determined using the Jahn-Teller effect illustrates a transition from cubic to tetragonal symmetry[9,10]. The cubic and hexagonal phases of $BaFeO_3$ studied by means of first-principle methods show ferromagnetic order[11]. Inorganic $CaFeO_3$ is used as a hole transport layer, offers superior stability and theoretical analysis validates the experimental results with a power conversion efficiency of ~16%[1]. Recent advancements have focused on enhancing the electrochemical and structural performance of $BaFeO_3$-based materials for energy applications. For instance, Co-doped $Ba_{0.95}La_{0.05}FeO_3-\delta$ (BLF) has recently been investigated as a promising cathode for protonic ceramic fuel cells (PCFCs) using a combined machine learning, Bayesian optimization, experimental, and DFT-based framework[12]. The study revealed that controlled doping can tune the oxygen vacancy formation energy and improve the material's electrochemical behavior and structural stability highlighting the multifunctional potential of $BaFeO_3$ derivatives. Similarly, $CaFeO_3$-based materials have shown excellent performance in energy storage applications. A recent study demonstrated that Mo-doped $CaFeO_3$ synthesized via a hydrothermal route exhibited a specific capacitance of 1722.5 F/g and strong cyclic retention over 5000 cycles when used in supercapacitor electrodes[13]. These findings emphasize the versatility of $CaFeO_3$ and motivate further theoretical investigation into its intrinsic electronic, magnetic, and structural characteristics an effort undertaken in the present study using first-principles methods. The selection of $BaFeO_3$ and $CaFeO_3$ arises from their rich physical phenomena involving Fe^{4+}/Fe^{3+} charge ordering, magnetic transitions, and perovskite distortions. These materials are known for their spin polarization, optical activity, and mechanical tunability. The motivation behind revisiting $BaFeO_3$ and $CaFeO_3$ lies in the lack of a comprehensive and comparative study employing multiple exchange-correlation functionals (GGA, mBJ-GGA, and YS-PBE0) to simultaneously evaluate structural, mechanical, magnetic, optical, and electronic properties. While these materials have been studied individually in the literature, there is a scarcity of integrated analysis correlating their half-metallicity, optical response, and elastic behavior, especially under hybrid functionals like YS-PBE0. Furthermore, this study explores their potential in spintronic and optoelectronic applications by examining their behavior up to high photon energies, which has not been previously reported in detail. This approach provides a broader understanding of their suitability for multifunctional device applications. We report in this investigation the ground state structural parameters, electronic nature, magnetic phase, optical and thermoelectric characteristics of $BaFeO_3$ and $CaFeO_3$ for advanced technological applications.

Computational details

Calculations have been performed using the density functional theory as implemented in the WIEN2K code[14] were explored for obtaining all results. The electronic exchange-correlation energy in the optimization of structural, electronic, optical, thermoelectric and vibrational properties of (Ba, Ca)FeO_3 perovskites is treated using the generalized gradient approximation of Perdew, Burke, and Ernzerhof (PBE-GGA)[15] and the modified Becke-Johnson exchange potential (mBJ-GGA)[16]. The computational parameters reported in Table 1 include the plane wave cutoff parameter in the interstitial region (RMT×Kmax), the muffin-tin radius (RMT), the maximum plane wave vector (Kmax), and the k-point mesh used for integrations within the irreducible Brillouin zone. Self-consistency is achieved with an energy convergence criterion of 10^{-5} Ry. The use of multiple exchange-correlation functionals was essential to ensure accurate and reliable predictions. GGA was employed as a baseline functional for structural and mechanical properties. The mBJ-GGA functional is known for improving the estimation of electronic band gaps in semiconductors, while the YS-PBE0 (a hybrid functional similar to HSE06) incorporates non-local exchange, offering more accurate magnetic and electronic structure predictions. This comparative approach allows us to assess the sensitivity of results to the functional and strengthens the reliability of the conclusions. the charge convergence was set to 10^{-4} e. The muffin-tin radii (RMT) were carefully selected to minimize sphere overlap and were as follows: Ba = 2.50 Å, Ca = 2.30 Å, Fe = 2.00 Å for $BaFeO_3$ and 1.82 Å for $CaFeO_3$, and O = 1.72 Å and 1.57 Å respectively. The plane wave cutoff parameter RMT×Kmax was chosen as 8.5 for $BaFeO_3$ and 9.0 for $CaFeO_3$. Wavefunctions inside the muffin-tin spheres were expanded in spherical harmonics up to lmax = 10. Valence electrons were treated semi-relativistically, and core electrons were treated fully relativistically. All calculations were carried out until total energy differences were less than 10^{-5} Ry between successive iterations. Inside the muffin-tin spheres, wave functions, electron charge densities, and potentials are expanded in spherical harmonics up to angular momentum l_{max} = 10, whereas plane waves are used in the interstitial regions.

Results and discussions

Structural analysis

(Ca, Ba)FeO_3 perovskites crystallize in the cubic $Pm\,\overline{3}m$ space group. (Ca^{2+}, Ba^{2+}) are bonded to twelve equivalent O^{2-} atoms to form (Ca, Ba)O_{12} cuboctahedra that share corners with twelve equivalent (Ca, Ba)O_{12} cuboctahedra, faces with six equivalent (Ca, Ba)O_{12} cuboctahedra, and faces with eight equivalent FeO_6 octahedra. (Ca, Ba) atoms occupy 1b (1/2, 1/2, 1/2), Fe atom are 1a (0, 0, 0) and O are located at 3d (1/2, 0, 0). The schematic crystal structure of (Ba, Ca)FeO_3 is visualized in Fig. 1.

	$R_{MT}K_{max}$	R_{MT} (Å)	R_{MT} (Fe)	R_{MT} (O)	k-points
$BaFeO_3$	8.5	2.50	2.0	1.72	1000
$CaFeO_3$	9	2.30	1.82	1.57	1000

Table 1. $R_{MTx}K_{max}$, R_{MT} for each component, and k-point using GGA for $BaFeO_3$ and $CaFeO_3$. (k-points = 10000) for optical properties. (k-points = 5000) for elastic properties.

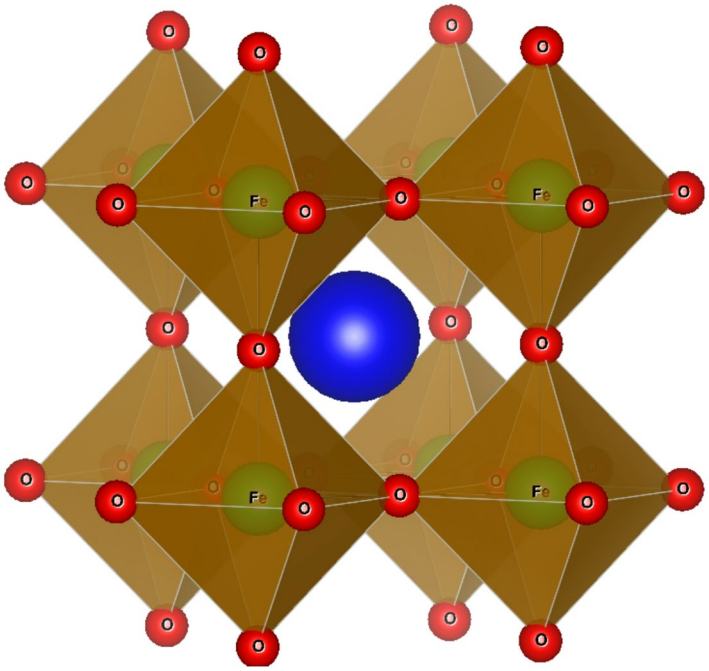

Fig. 1. Schematic crystal structure of $BaFeO_3$ perovskite.

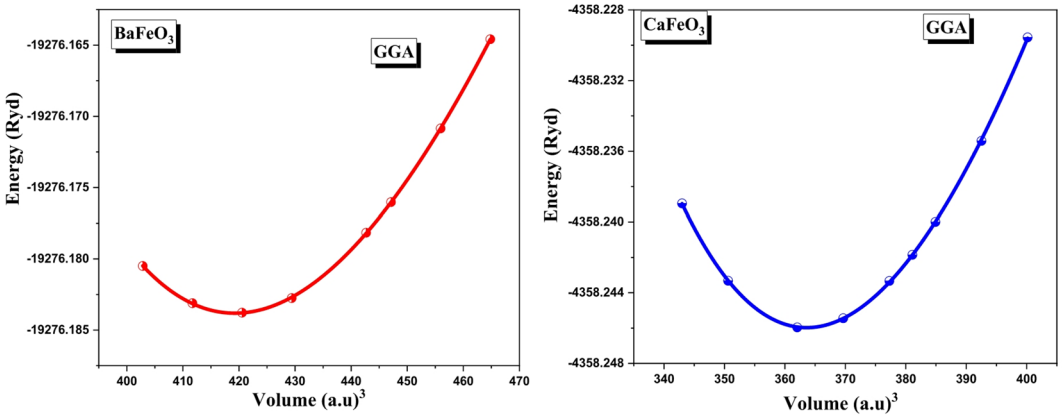

Fig. 2. Calculated energy vs. volume curves for optimizing $BaFeO_3$ and $CaFeO_3$ using GGA.

The formation energy as a function of volume in ferromagnetic state for (Ca, Ba)FeO_3 (Fig. 2), present in the negative formation energy indicates that these perovskites are energetically stable and could be synthesized experimentally under ambient conditions. The lattice constant, bulk modulus and its pressure derivative is estimated from the optimum volume of the unit cell as shown in Table 2. The pressure derivative of the bulk modulus (B′) provides insight into how the material's resistance to compression evolves under external pressure. A higher value of B′ indicates that the material becomes significantly stiffer when compressed, reflecting a strong interatomic interaction response to pressure. In contrast, a lower B′ implies a more gradual change in stiffness with pressure. This parameter is essential in understanding the mechanical resilience of perovskite structures under high-pressure conditions. The optimized lattice constants of the cubic unit cell $CaFeO_3$ and $BaFeO_3$ are in good agreement with the experimental values of 3.77 Å and 3.971 Å[3,8,17,18]. Our lattice constants of $CaFeO_3$ and $BaFeO_3$ agree well with theoretical values reported in the literature[2,19]. Bond lengths in molecular crystals depend primarily on the nature of the elements involved and the number of bonding electron pairs minus the number of antibonding electron pairs. It should be noted that the present study assumes ideal stoichiometric structures for $BaFeO_3$ and $CaFeO_3$. The potential influence of oxygen vacancies and Fe^{4+}/Fe^{3+} charge disproportionation, which are known to affect structural and electronic behavior in perovskites, was not considered in the current calculations. The calculated bond lengths between different atoms for $CaFeO_3$ and $BaFeO_3$ are listed in Table 2. The Goldschmidt tolerance factor t was calculated using the conventional expression[20]:

	a_0 (Å)	B (GPa)	B′	E_0 (Ry)	Bond lengths (Å)
$BaFeO_3$ Theor. Exp.	3.9656 4.015[20] 3.971[8,18,19]	138.34 124.70[3] 167.6[4]	3.335 4.59[5]	− 19276.184117	Fe-O = 1.982 Ba-O = 2.804 Ba-Fe = 3.4343
CaFeO3 Theor. Exp.	3.777 3.72[2] 3.77[20]	157.51 178.30[2]	4.758 4.640[2]	− 4358.245975 − 4352.7724[2]	Fe-O = 1.888 1.860[2] Ca-O = 2.6707 2.630[2] Ca-Fe = 3.2709 3.211[2]

Table 2. Lattice constant, bulk modulus and its pressure derivative, the minimum energy E_0 and bond lengths for $BaFeO_3$ and $CaFeO_3$.

$$t = \frac{r_A + r_o}{(r_B + r_o) \times \sqrt{2}}$$

where r_A, r_B, and $r_O$are the ionic radii of the A-site cation (Ba^{2+} or Ca^{2+}), B-site cation (Fe^{4+}), and the oxygen anion (O^{2-}), respectively. This factor provides a qualitative assessment of the geometric stability of the perovskite structure. The calculated tolerance and octahedral factors for $CaFeO_3$ and $BaFeO_3$ are (1.0002 and 0.349) and (1.0004 and 0.416). The tolerance and octahedral factors are lyingin the range (1.0004–1.04) and 0.47, which confirm their structural stability[21,22]. The chemical reaction of formation of (Ba, Ca)FeO_3 from their elementary components can be defined as:

$$(Ba, Ca)_{(s)} + Fe_{(s)} + \frac{3}{2}O_{2_{(g)}} \rightarrow (Ba, Ca)FeO_{3_{(s)}} \tag{1}$$

The Gibbs free energy of reaction of equation:

$$\Delta G_f^0 = G_{(BaFeO_3)}^0 - G_{(Ba)}^0 - G_{Fe}^0 - \frac{3}{2}G_{O_2}^0 \tag{2}$$

$$\Delta G_f^0 = G_{(CaFeO_3)}^0 - G_{(Ca)}^0 - G_{Fe}^0 - \frac{3}{2}G_{O_2}^0 \tag{3}$$

where G^0 is the standard Gibbs free energy of the substances involved in the reaction and is expressed as:

$$G^0 = E^{DFT} + ZPE - TS^0 \tag{4}$$

where E^{DFT} is the total energy obtained from the DFT calculations, ZPE is the zero-point energy estimated from vibration analyses, and TS^0 is the product of temperature and entropy at T = 298.15 K. The formation energy of $BaFeO_3$ and $CaFeO_3$ per atom is -5.56 eV and − 5.71 eV respectively. Although phonon dispersion calculations were not performed in this study, the significantly negative formation energies obtained for $BaFeO_3$ (− 5.56 eV/atom) and $CaFeO_3$ (− 5.71 eV/atom) provide strong evidence of their thermodynamic stability under equilibrium conditions. These values suggest that both materials are energetically favorable and could be synthesized experimentally. Similar computational approaches involving formation energy and phonon dispersion to assess the structural and dynamic stability in oxide compounds have been successfully demonstrated in recent studies, such as that by Amira Nour Asfora et al.[23]. The relevance of phonon dispersion and cohesive energy analysis in determining structural stability has also been highlighted in similar oxide systems such as $ZrSi_3O_8$ and Zr_3SiO_8, as reported by M. Ould Moussa et al.[24]. In the context of rare-earth and transition-metal perovskites, first-principles studies like that of Slimane Haid et al.[25] have shown how combining formation energy with GGA + U corrections can reveal both structural and magnetic stability. Furthermore, the integration of phonon analysis, tolerance factor, and structural parameters to assess the thermodynamic stability of double perovskites has also been effectively demonstrated in the work on Ba_2DyTaO_6 by Slimane Haid et al.[26].

Elastic constants and mechanical characteristics

The three elastic constants C_{11}, C_{12} and $C_{44}$and bulk modulus for $BaFeO_3$ and $CaFeO_3$ with cubic symmetryare calculated using the nonlinear Charpin method[27]. We note that all elastic moduli verify the stability criteria, hence their mechanical stability[20].

$$0 \prec C_{11}, 0 \prec C_{44}, 0 \prec C_{11} - C_{12}, 0 \prec C_{11} + 2C_{12}, C_{12} \prec B \prec C_{11}$$

The mechanical properties of $BaFeO_3$ and $CaFeO_3$, including shear modulus, bulk modulus, anisotropy factor, Young's modulus, Poisson's ratio, and the B_H/G_H ratio calculated using the Voigt, Reuss, and Hill approximations, are presented in Table 3. The shear and bulk moduli of $BaFeO_3$ are higher than those of $CaFeO_3$, indicating that $BaFeO_3$ is both harder and stiffer. Both perovskites exhibit significant anisotropy. Additionally, Young's modulus confirms that $BaFeO_3$ has a greater resistance to uniaxial deformation compared to $CaFeO_3$. Poisson's ratio, which measures the ratio of transverse to longitudinal strain, has values greater than 0.25 for both materials, suggesting that the dominant interatomic forces are of a central nature. The B/G ratio serves as an indicator of ductility,

	$BaFeO_3$	$CaFeO_3$
C_{11} (GPa)	202.67	184.75
C_{12} (GPa)	98.05	101.29
C_{44} (GPa)	109.17	82.46
C_{11} - C_{12}	104.61	83.46
G_v (GPa)	86.42	66.17
G_R (GPa)	76.08	59.30
G_H (GPa)	81.25	62.73
B_H (GPa)	132.93	129.11
A	2.08	1.97
E_V (GPa)	213.09	169.54
E_R (GPa)	191.68	154.29
E_H (GPa)	202.50	161.97
ϑ_V	0.23	0.28
ϑ_R	0.25	0.30
ϑ_H	0.24	0.29
B_H/G_H	1.63	2.05

Table 3. Elastic constants, shear moduli, bulk modulus, anisotropy factor, young's moduli, poisson's ratios and B_H/G_H ratio for $BaFeO_3$ and $CaFeO_3$.

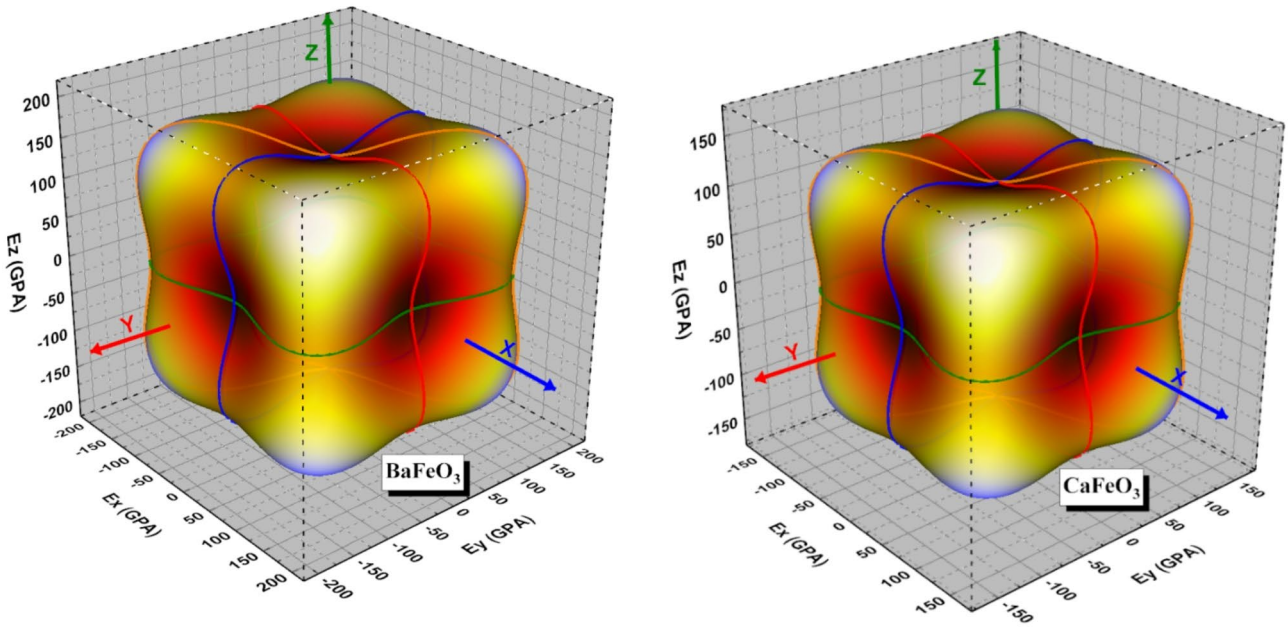

Fig. 3. 3D surface of Young's modulus for $BaFeO_3$ and $CaFeO_3$.

where values above 1.75 correspond to ductile behavior and values below indicate brittleness. Based on this criterion, $BaFeO_3$ is ductile, while $CaFeO_3$ is brittle. It is also noteworthy that the bulk modulus lies between the shear modulus and Young's modulus for both compounds, implying that these materials accommodate uniaxial deformation more readily than volumetric compression. Figures 3 and 4 display the 3D and 2D distributions of Young's modulus (E) for $BaFeO_3$ and $CaFeO_3$. In both materials, Young's modulus reaches its maximum along the z-axis (E_{max} = 125 GPa for $BaFeO_3$ and 100 GPa for CaFeO3) and its minimum along the x-axis (E_{min} = 80 GPafor $BaFeO_3$ and 50 GPa for $CaFeO_3$). This results in elastic anisotropy factors ($A_E = E_{max}/E_{min}$) of 1.56 and 2.

Electronic properties

Spin gapless semiconductors are a class of materials, where band structure presents no band gap for one spin channel while there is a finite band gap in another spin channel. Although the concept of spin gapless semiconductors (SGS) refers to materials that exhibit a true zero band gap in one spin channel and a finite gap in the other, the present results do not strictly fulfill this criterion. In our calculations using mBJ-GGA and YS-PBE0, $BaFeO_3$ and $CaFeO_3$ show a metallic character in the spin-up channel and a narrow indirect band gap

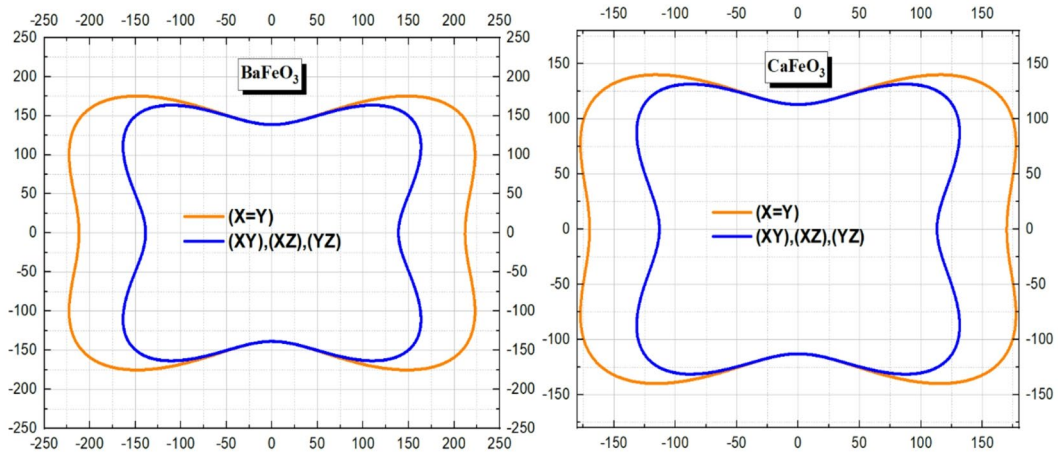

Fig. 4. 2D surface of Young's modulus for $BaFeO_3$ and $CaFeO_3$.

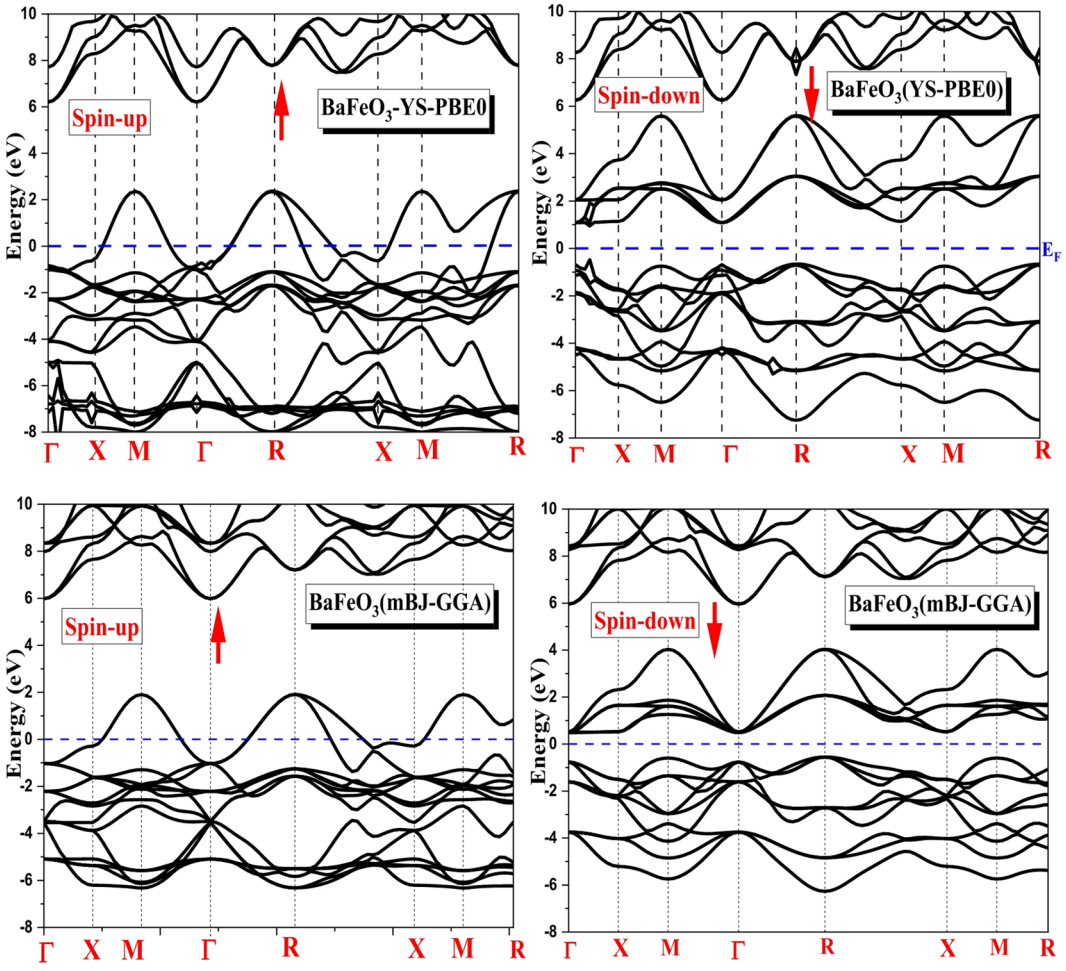

Fig. 5. Band structure of $BaFeO_3$ using spin-up and spin-dn using mBJ-GGA and YS-PBE0.

(~ 1.0–1.7 eV) in the spin-down channel. Therefore, these compounds can be more appropriately described as exhibiting spin-polarized semiconducting behavior, rather than being classified as ideal SGS materials. Figures 5 and 6 show spin-up (left panel) and spin-down (right panel) band structure of $BaFeO_3$and $CaFeO_3$ using YS-PBE0 and mBJ-GGA approximations. For the spin-up and using YS-PBE0 and mBJ-GGA, both perovskites under study have a metallic character, while, they show an indirect M-Γ band gap for the spin-dn. The electronic

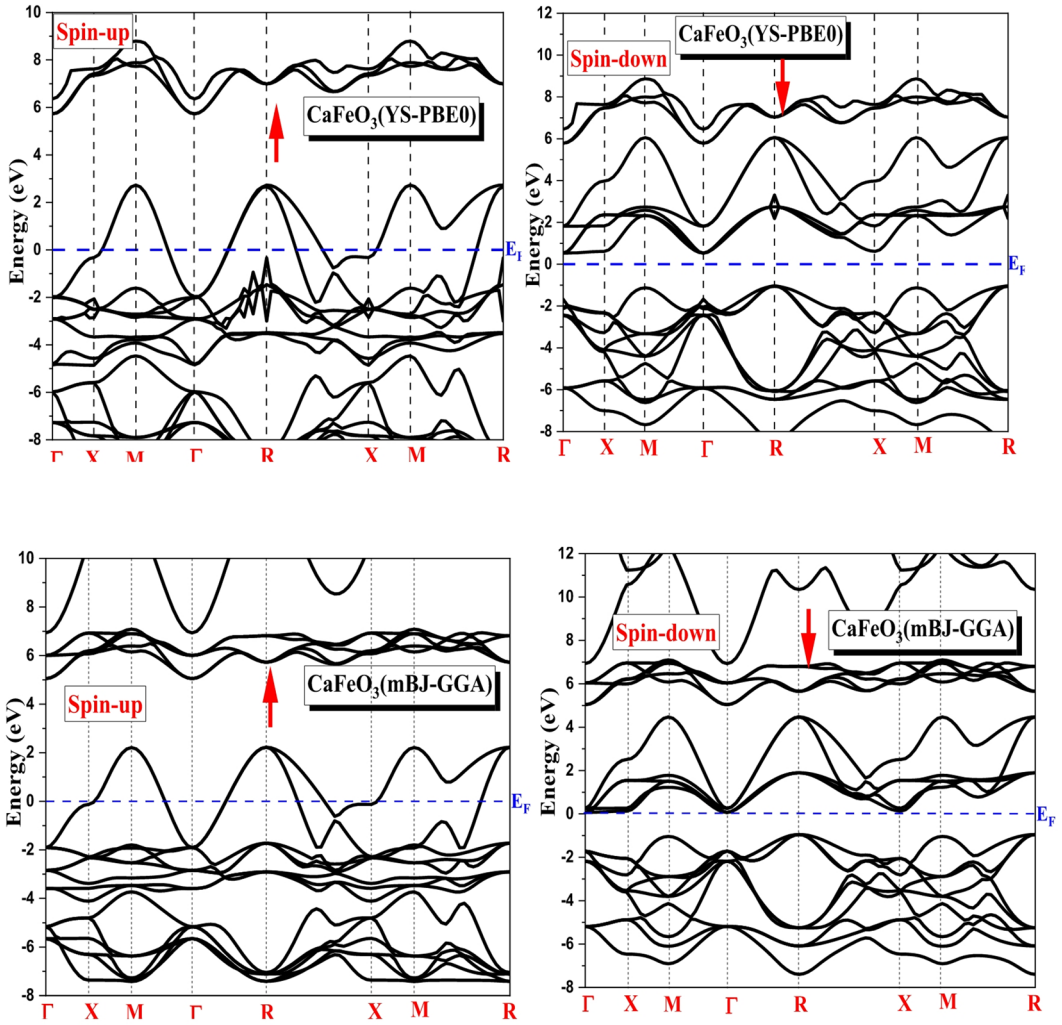

Fig. 6. Band structure of $CaFeO_3$using spin-up and spin-dn using mBJ-GGAandYS-PBE0.

	GGA		mBJ-GGA		YS-PBE0(HSE06)	
	Spin-up	Spin-dn	Spin-up	Spin-dn	Spin-up	Spin-dn
BaFeO3	Metal	Metal	Metal	1.03	Metal	1.74
CaFeO3	Metal	Metal	Metal	1.01	Metal	1.55

Table 4. Band gap of $BaFeO_3$ and $CaFeO_3$ using GGA, Mbj-GGA and YS-PBE0(HSE06).

and magnetic characteristics of a ferromagnetic material depend on the spin states, and the energy difference is adopted in the electronic transitions between orbits. The different band gaps of $BaFeO_3$ and $CaFeO_3$ perovskites are reported in Table 4. In the case of the spin-up state, the valence band crosses the Fermi level and enters into the conduction band, so $BaFeO_3$and $CaFeO_3$ are metallic. For the spin-down, a narrow indirect M-Γ band gap of 1.03 eV and 1.01 eV (1.74 eV and 1.55 eV) is found for mBJ-GGA (YS-PBE0(HSE06)). In the GGA case, both compounds are metallic in both spins. The electronic contribution in the band structure is explained by the total and partial spin-polarized densities of states (DOS and PDOS), as illustrated in Fig. 7. The electronic contribution in the valence band located between (-0.5 eV and − 2.5 eV) and (-4.5 eV and − 6 eV) is mainly due to Fe-3d and O-2p electrons. Hybridization of the O-2*p* and Fe-3*d* states is noted in the upper of the valence band in the spin-up states, as well as in the spin-down state, this makes $BaFeO_3$ and $CaFeO_3$ metallic. The conduction band is empty for the spin-up. In the case of spin-down and mBJ-GGA functional, polarization occurs at the Fermi level and Fe-3d jumps into conduction band, accordingly a narrow band gap of 1.03 eV and 1.01 eV exists between the valence and conduction band for $BaFeO_3$and $CaFeO_3$. For the spin-down channel of $CaFeO_3$, a narrow indirect band gap (~ 1.01–1.55 eV) appears between the M and Γ points under the mBJ-GGA and YS-PBE0 functionals, while the spin-up channel remains metallic. This indicates spin-polarized semiconducting behavior rather than a fully metallic state. Figures 8 and 9 show the electronic densities of states of Ba (s, p), Ca (p, d, d-eg, d-t2g), Fe

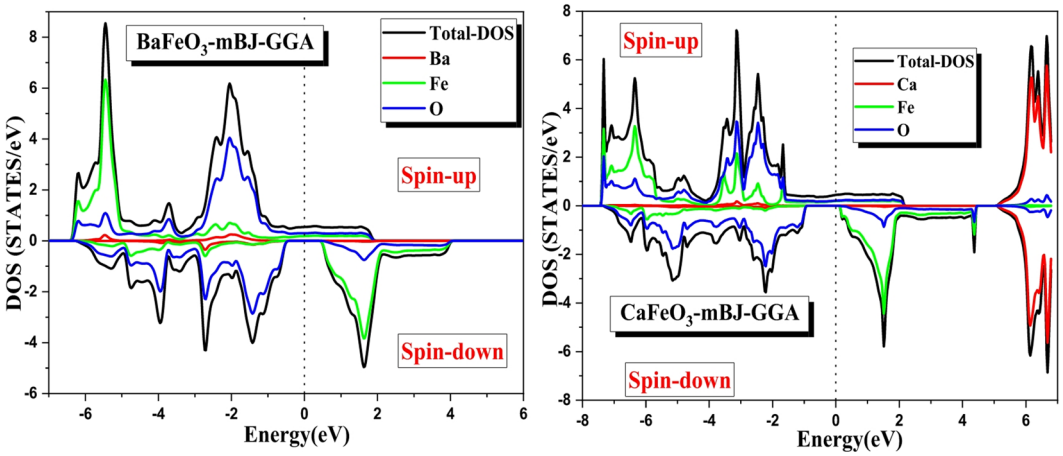

Fig. 7. The density of states for $BaFeO_3$ and $CaFeO_3$ using mBJ-GGA.

(s, p, d, d-eg, d-t2g) and O (s, p) for $BaFeO_3$and $CaFeO_3$with both spin and using mBJ-GGA approach. Local octahedral coordination of Fe (3d) and Ca (3d) for both spin give two degenerate orbitalsd-eg and d-t2g. The tetrahedral and octahedral symmetries play a crucial role in stabilizing the ordering of the transition metal (Fe) in BaFeO3 and CaFeO3. The resulting crystal field causes the Fe 3d orbitals to split into two distinct sets of non-degenerate states, t2g and e.g., as depicted in Figs. 8 and 9. In this splitting, the e.g. doublet lies at a lower energy level than the t2g triplet. The six electrons are arranged such that the wave functions of the 3d e.g. doublet exhibit weak hybridization with the oxygen 2p orbitals. In contrast, the 3d t2g states strongly hybridize with the oxygen 2p orbitals, forming bonding and antibonding states. The Fe 3d states are occupied so that the t2g orbitals are filled for both spin-up and spin-down electrons, while the e.g. and t2g orbitals remain unoccupied for both spin channels. The bonding nature in both $BaFeO_3$ and $CaFeO_3$ exhibits a mixed ionic–covalent character. The Fe–O bonds show significant covalent behavior due to the overlap between Fe 3d and O 2p orbitals, as reflected in the electronic density of states (DOS) and partial charge density maps. On the other hand, Ba–O and Ca–O bonds possess more ionic features, attributed to the large electronegativity difference between Ba/Ca and O. This hybrid bonding nature contributes to the structural flexibility and multifunctional electronic behavior of these perovskite oxides. It is important to emphasize that under GGA functional, both spin channels demonstrate metallic behavior, which further supports the interpretation that these materials are not true spin gapless semiconductors. Instead, their spin-resolved electronic features suggest potential use in spintronic devices due to their asymmetrical spin band structures under advanced functionals. Recent studies have demonstrated that including spin–orbit coupling (SOC) and modified Becke–Johnson (TB-mBJ) functionals significantly alters the electronic structure and band gaps of perovskite materials. A comprehensive investigation on 40 novel AMX_3 compounds revealed how the combined influence of SOC and TB-mBJ can tailor the band structure, which is essential in tuning perovskite-based materials for electronic and optoelectronic applications. These insights support our use of hybrid and mBJ functionals in exploring the electronic behavior of (Ba, Ca)FeO_3[28].

Magnetic properties

Density functional theory (DFT) calculations were conducted using the GGA, mBJ-GGA, and YS-PBE0 approximations to investigate the magnetic properties of BaFeO3 and CaFeO3 perovskites. The magnetic moment originates from both the constituent atoms and the interstitial regions. Both $BaFeO_3$ and $CaFeO_3$ display ferromagnetic behavior, with the primary contribution to magnetization arising from the partially filled Fe 3d orbitals. Table 5 presents the interstitial, atomic, and total magnetic moments for these compounds calculated with the three functionals. Notably, the mBJ-GGA method yields higher magnetization values compared to YS-PBE0 and GGA. The total magnetic moments obtained with mBJ-GGA and YS-PBE0 are integer values (4 μB), consistent with the half-metallic nature of these materials. Half-metallic ferromagnetism and spin polarization effects, similar to those observed in Fe(Mn)-doped nitrides like CdN and ZnN, have also been reported using FP-LAPW methods[29]. These findings support our interpretation of strong p–d hybridization in (Ba, Ca)FeO_3 systems as a key factor driving their spin-polarized magnetic behavior. A similar trend was reported for PdO, where GGA predicted metallic behavior in both spin channels, but upon inclusion of a Hubbard U correction (GGA + U), half-metallic ferromagnetism emerged[30]. This highlights how strong electron correlation and exchange interactions, as modeled by GGA + U or hybrid functionals, can critically influence magnetic behavior and spin polarization consistent with our observations in (Ba, Ca)FeO_3. The O 2p bands at the Fermi level are partially unoccupied in the spin-up channel and fully unoccupied in the spin-down channel. It is observed that stronger hybridization between O 2p and Fe 3d orbitals tends to reduce the magnetic moment. Experimentally, the magnetic moment of Fe in CaFeO3 is reported as 3.5 μB at 15 K[6]. The direction of the interstitial magnetization aligns with that of Fe 3d and O 2p magnetizations for all functionals and both compounds, while for the mBJ-GGA functional, the magnetic moments of Ba and Ca are antiparallel to that of Fe. The calculated magnetic moments for Fe atoms (3.5–4.0 μB) are in good agreement with experimental reports, such as the 3.5 μB measured in $CaFeO_3$ at 15 K[6]. Additionally, the use of hybrid functionals improved the accuracy of band

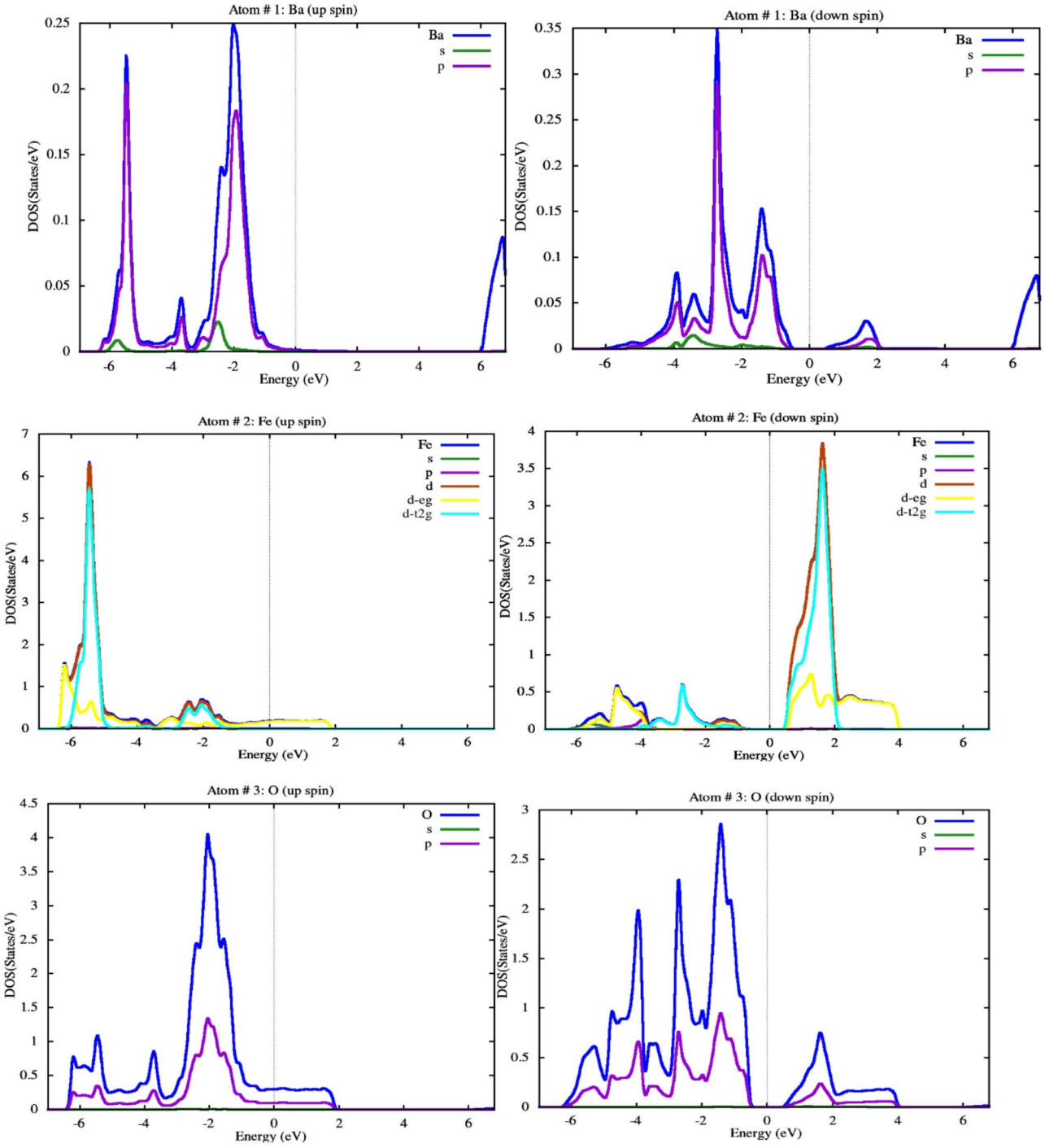

Fig. 8. Partial density of states (PDOS) for $BaFeO_3$ using mBJ-GGA.

gap predictions, although direct experimental band gap values remain limited in the literature for a reliable one-to-one comparison. It is important to note that in half-metallic ferromagnets, the total magnetic moment per formula unit is expected to be an integer value, which is a signature of the complete spin polarization at the Fermi level. This behavior follows the Slater–Pauling rule, which relates the total magnetic moment (in μB) to the number of valence electrons (Z_t) through the relation: $M_t = Z_t - 24$, for transition-metal-based half-metallic systems. The integer nature of the magnetic moment arises because one spin channel (usually spin-down) has a semiconducting gap, while the other (spin-up) remains metallic, leading to complete spin asymmetry at the Fermi level. In our study, the calculated total magnetic moments of $BaFeO_3$ and $CaFeO_3$ (4.0 μB and 3.0 μB, respectively) conform to this expectation under the mBJ-GGA and YS-PBE0 functionals, reinforcing their half-metallic nature, For $BaFeO_3$, Z_t is calculated as follows: Ba contributes 2 valence electrons ($6s^2$), Fe contributes 8 ($3d^6\ 4s^2$), and each oxygen atom contributes 6 electrons; hence, $Z_t = 2\ (Ba) + 8\ (Fe) + 3 \times 6\ (O) = 28$. Applying

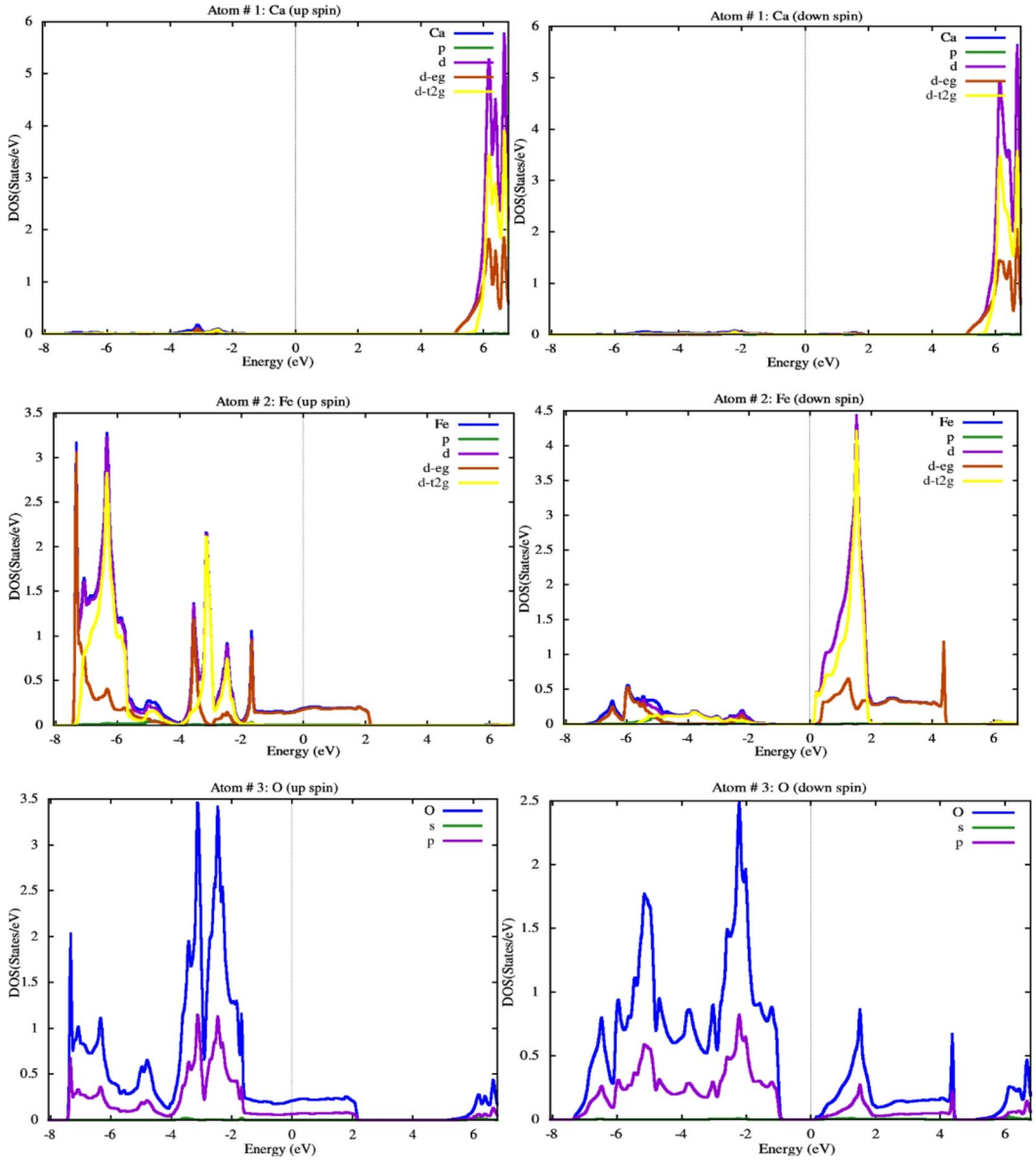

Fig. 9. Partial density of states (PDOS) for $CaFeO_3$ using mBJ-GGA.

	Functional	$M_{interstitial}$ (μB)	M_A (μB)	M_{Fe} (μB)	M_O (μB)	M_{Total} (μB)
$BaFeO_3$	GGA	0.151	0.015	3.006	0.173	3.694 Exp. 3.5[8]
	mBJ-GGA	0.008	− 0.001	3.607	0.129	4.001 4.01[9]
	YS-PBE0	0.144	0.011	3.746	0.03232	3.999
$CaFeO_3$	GGA	0.166	0.012	2.750	0.149	3.378
	mBJ-GGA	0.031 0.170[2]	− 0.008 0.0115[2]	3.519 3.6843[2]	0.153 0.0451[2]	4.00 4.00[2]
	YS-PBE0	0.185	0.010	3.602	0.0671	3.999

Table 5. Interstitial, atomic and total magnetic moment for$BaFeO_3$ and $CaFeO_3$using GGA, mBJ-GGA and YS-PBE0 functionals.

the rule gives $M_t = 28 - 24 = 4$ μB, which is in excellent agreement with our calculated total magnetic moment. This confirms the half-metallic nature of $BaFeO_3$ and supports its potential use in spintronic applications. A similar analysis for $CaFeO_3$ yields $Z_t = 2$ (Ca) + 8 (Fe) + 18 (O) = 28, and hence $M_t = 4$ μB as well, matching our computational results.

Optical characteristics

The optical study of $BaFeO_3$ and $CaFeO_3$ perovskites through their characteristics such as absorption, energy loss, real and imaginary dielectric constants, refractive index, extinction coefficient, real optical conductivity and optical reflectivity are visualized in Fig. 10. Figure 10 consists of eight subplots labeled (a) to (h), showing: (a) absorption coefficient, (b) energy loss function, (c) real part of dielectric function, (d) imaginary part, (e) refractive index, (f) extinction coefficient, (g) real optical conductivity, and (h) reflectivity. All plots have their axes clearly labeled, and the photon energy is shown on the x-axis in units of eV. Parallel polarized absorption peaks are observed in these perovskites. For photon energy between 15 eV and 30 eV, the absorption is more pronounced, this results in a decrease in light transmission. $BaFeO_3$ and $CaFeO_3$ exhibit large absorption coefficients 350×10^4 cm^{-1} and 500×10^4 cm^{-1} in the ultraviolet range attributed to the infrared phonon mode.

A higher absorption coefficient (α) implies that incident light is strongly attenuated within a short distance inside the material. This means that a significant portion of the incident optical power is absorbed per unit thickness, making materials with large α values particularly suitable for energy harvesting and optoelectronic devices. The absorption coefficient is directly related to the imaginary part of the dielectric function and governs how quickly the intensity of light decays as it propagates through the medium, according to Beer–Lambert's law $I(x) = I_0.e^{-\propto .x}$ where I(x) is the intensity at depth x, and I_0 is the initial intensity. The loss energy is not important at visible and ultraviolet light for perovskites under study. The high absorption coefficient at ultraviolet region, low reflectivity near infrared region, the narrow band gap semiconducting nature for the spin-dn make these materials suitable for optoelectronic applications. The real part specifies the degree of polarization, it is more important in the visible region. The static dielectric constant traduces its ability to store electrical energy in low frequency. The static real dielectric constant for $BaFeO_3$ and $CaFeO_3$ is 9 and 7.7. The real part of the dielectric function becomes negative between 3 and 3.5 eV photon energy. This explains that the displacement vector and the electric field vector are opposite. The large static dielectric constant translates the high degree of polarization and points to the ferroelectric behavior of these materials. The imaginary part is associated with dielectric losses. The first peak of the imaginary dielectric function located in the energy about 2.5 eV corresponds to the drop of the real part of the dielectric function. The refractive index of a material determines the extent to which light bends as it passes through the material. The high static refractive index for $BaFeO_3$ and $CaFeO_3$ (3 and 2.75) limits the efficiency of solar cells. The observed refractive index values below unity at high photon energies are attributed to artifacts of DFT-based optical calculations and should not be interpreted as evidence of superluminal behavior. The extinction coefficient determines the degree to which light is absorbed or reflected at a particular wavelength. The maximum extinction coefficient for these materials is about 2. The real part of the optical conductivity contains the same information as the imaginary part of the dielectric function. The maximum real optical conductivity for $BaFeO_3$ and $CaFeO_3$ is 12,500 $(\Omega.\ cm)^{-1}$ and 17,500 $(\Omega.\ cm)^{-1}$ obtained at ultraviolet region.The real optical conductivity exhibits a prominent sharp peak at around 2.5 eV, attributed to the transition from O-2p orbitals from the valence band to the conduction band. Optical reflectivity refers to the phenomenon where light waves bounce back and forth as they pass from one material to another with different properties. The static optical reflectivity for $BaFeO_3$ and $CaFeO_3$ is around 0.25 and 0.22. The optical reflectivity of a solar device is a key parameter of its efficiency. The optical response of $BaFeO_3$ and $CaFeO_3$ is closely related to their electronic structure. In particular, the strong absorption in the UV region and the high values of the real and imaginary parts of the dielectric function originate from interband transitions. These transitions primarily occur between the O 2p states in the valence band and Fe 3d states in the conduction band. The onset of optical absorption corresponds to the energy difference between these states, which explains the position of absorption edges. Moreover, the sharp peaks in the optical conductivity and refractive index spectra can be attributed to direct electronic transitions near high-symmetry points in the Brillouin zone. Such transitions are influenced by the density of states and the spin-polarized band structures, which reflect the strong hybridization between O and Fe orbitals. This light–matter interaction is essential for understanding the potential use of these materials in UV and spin-dependent optoelectronic applications. While experimental optical spectra for $BaFeO_3$ and $CaFeO_3$ are scarce, the calculated static dielectric constants (~ 9 and ~ 7.7) and high absorption coefficients (~ 10^4–10^5 cm^{-1}) are comparable in magnitude to values reported for similar perovskite oxides[31]. Further experimental studies would help to validate and refine these predictions. Similar DFT-based optical investigations on related telluride systems have shown that spin–orbit coupling significantly influences optical transitions near the Fermi level, as reported for GeTe and SnTe[32]. This further emphasizes the sensitivity of optical properties to band structure modifications, particularly in narrow-gap or spin-polarized materials. Similar optical spectral profiles have been observed in related oxide systems such as $BiGaO_3$, where both mBJ-GGA and EV-GGA functionals yielded comparable absorption features and enhanced band gap predictions[33]. These results reinforce the reliability of using mBJ-GGA for studying the optical transitions and electronic excitations in perovskite-like oxides.

Phonon properties

To further confirm the dynamical stability of $BaFeO_3$ and $CaFeO_3$, we have calculated the phonon dispersion relations along the high-symmetry directions of the Brillouin zone together with the phonon density of states (PDOS), as shown in Fig. 11. For both compounds, the absence of imaginary frequencies throughout the Brillouin zone clearly indicates their dynamical stability. In $BaFeO_3$, the phonon spectrum extends up to ~17 THz, with the low-frequency region dominated by vibrations of the heavier Ba atoms, while the intermediate range is mainly contributed by Fe atoms. The high-frequency optical modes are primarily associated with the

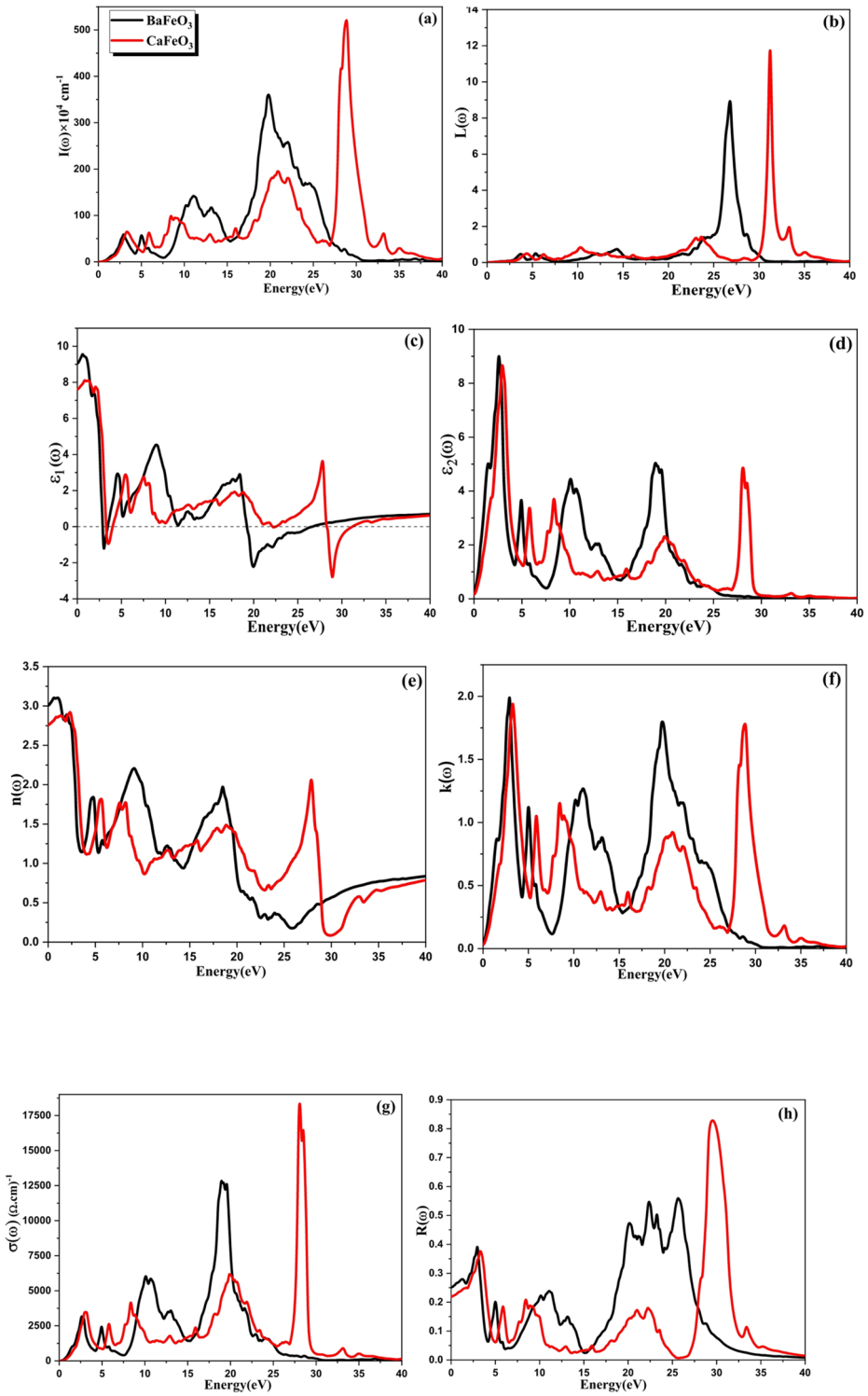

Fig. 10. Absorption coefficient (**a**), energy loss (**b**), real (**c**) and imaginary (**d**) components of the dielectric function, refractive index (**e**), extinction coefficient (**f**), the real optical conductivity (**g**) and reflectivity (**h**) as functions of photon energy for $BaFeO_3$ and $CaFeO_3$perovskites using mBJ-GGA.

O vibrations, as evidenced by the PDOS. Similarly, for $CaFeO_3$, the phonon frequencies reach ~ 18 THz, with Ca contributing mainly in the low-frequency acoustic modes, while Fe and O dominate the mid- and high-frequency regions, respectively.

The separation between acoustic and optical branches is more pronounced in $CaFeO_3$ due to the lighter mass of Ca compared to Ba. The strong hybridization between Fe and O modes in the optical region highlights the covalent nature of the Fe–O bonding, which plays a key role in the electronic and magnetic properties of

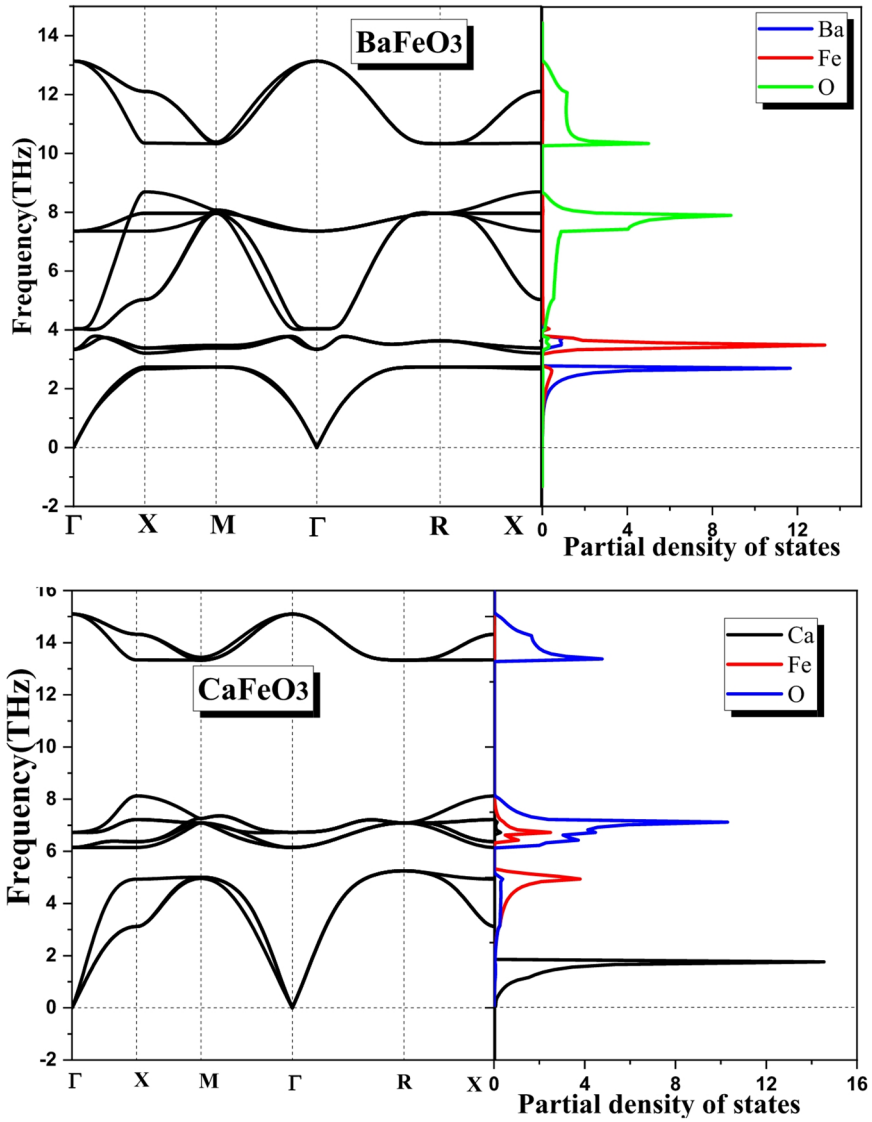

Fig. 11. Phonon dispersion curves and partial phonon density of states (PDOS) for $BaFeO_3$ and $CaFeO_3$.

these perovskites. Overall, the phonon results complement the negative formation energies reported earlier, confirming both the thermodynamic and dynamical stability of $BaFeO_3$ and $CaFeO_3$. These findings reinforce the reliability of our theoretical predictions regarding their electronic, magnetic, and optical characteristics, and further support their potential for spintronic and optoelectronic applications.

Conclusion

Theoretical investigations of the cubic perovskites $BaFeO_3$and $CaFeO_3$were carried out using the full-potential linearized augmented plane-wave method implemented in the Wien2k code. Analysis of the tolerance and octahedral factors, formation energies, phonon dispersion and elastic moduli confirms the structural, dynamical, and mechanical stability of both compounds. $BaFeO_3$ and $CaFeO_3$ display ferromagnetic behavior, primarily driven by the unfilled Fe 3d orbitals. The Fe 3d t2g states strongly hybridize with O 2p states, resulting in bonding and antibonding interactions. The total magnetic moment for both materials, calculated using mBJ-GGA and YS-PBE0 functionals, is an integer value of 4 μB, reflecting their half-metallic character. The Fe 3d orbitals are occupied such that the t2g states are filled in both spin-up and spin-down channels, while the e.g. and t2g states remain unoccupied for both spins. Additionally, these materials exhibit a high absorption coefficient in the ultraviolet region, low reflectivity in the near-infrared range, and a narrow band gap semiconductor behavior in the spin-down channel, making them promising candidates for optoelectronic applications.Based on the calculated magnetic, optical, and electronic properties, both $BaFeO_3$ and $CaFeO_3$ show promising potential for use in spintronic and ultraviolet optoelectronic applications. Their strong spin polarization, high absorption coefficients in the UV region, and robust structural stability suggest applicability in devices such as spin-filters, photodetectors, and memory elements. Future studies could explore the effects of oxygen vacancies, mixed

valence states, and spin–orbit coupling (SOC) on the physical behavior of these compounds. Experimental validation of the electronic and optical predictions is also recommended to assess their practical viability.

Data availability

Data underlying the results presented in this paper are not publicly available at this time but may be obtained from the corresponding author (fatmimessaud@yahoo.fr) upon reasonable request.

Received: 27 May 2025; Accepted: 18 September 2025
Published online: 23 October 2025

References

1. Lotey, G. S. et al. Potential of low-cost inorganic CaFeO3 as transporting material for efficient perovskite solar cells. *Mater. Today Commun.* **35**, 105956. https://doi.org/10.1016/j.mtcomm.2023.105956 (2023).
2. Ali, Z., Ahmad, I., Khan, B. & Khan, I. Robust Half-Metallicity and magnetic properties of cubic perovskite CaFeO3. *Chin. Phys. Lett.* **30**, 047504. https://doi.org/10.1088/0256-307X/30/4/047504 (2013).
3. Kanamaru, F. et al. Synthesis of a new perovskite CaFeO3. *Mater. Res. Bull.* **5**, 257–262 (1970).
4. Verma, A. S. & Kumar, A. Bulk modulus of cubic perovskites. *J. Alloys Compd.* **541**, 210–214. https://doi.org/10.1016/j.jallcomm.2012.07.027 (2012).
5. Fatmi, M. et al. Investigation of structural elastic electronic optical and thermoelectric properties of LiInS2 and LiInTe2 for optoelectronic and energy conversion. *Sci. Rep.* **15** (1), 27859. https://doi.org/10.1038/s41598-025-13916-1 (2025).
6. Woodward, P. M., Cox, D. E., Moshopoulou, E., Sleight, A. W. & Morimoto, S. Structural studies of charge disproportionation and magnetic order in CaFeO3. *Phys. Rev. B.* **62**, 844 (2000).
7. Matsuno, J. et al. Different routes to charge disproportionation in perovskite-type Fe oxides. *Phys. Rev. B.* **66**, 193103 (2002).
8. Hayashi, N. et al. BaFeO3: A ferromagnetic iron oxide. *Angew Chem.* **123**, 12755–12758. https://doi.org/10.1002/ange.201105276 (2011).
9. Cherair, I., Bousquet, E., Schmitt, M. M., Iles, N. & Kellou, A. First-principles study of strain-induced Jahn–Teller distortions in BaFeO3. *J. Phys. : Condens. Matter.* **30** (25), 255701. https://doi.org/10.1088/1361-648X/aac46d (2018).
10. Hoedl, M. F., Gryaznov, D., Merkle, R., Kotomin, E. A. & Maier, J. Interdependence of oxygenation and hydration in Mixed-Conducting (Ba,Sr)FeO3–δ perovskites studied by density functional theory. *J. Phys. Chem. C.* **124** (22), 11780–11789. https://doi.org/10.1021/acs.jpcc.0c01924 (2020).
11. Adeagbo, W. A. et al. Electronic and magnetic properties of BaFeO3 on the Pt(111) surface in a quasicrystalline approximant structure. *Phys. Status Solidi B.* **257** (7), 1900649. https://doi.org/10.1002/pssb.201900649 (2020).
12. Tahir, A. & Ciucci, F. Optimization of Co-Doped BaFeO3 cathodes for enhanced Pcfc performance: an integrated computational and experimental Approach, 2025 Meet. Abstr. MA2025-**01** 2252. (2025). https://doi.org/10.1149/MA2025-01412252mtgabs
13. Alyousef, H. A., Abdelmohsen, S. A. & Alqarny, A. S. Specifying the mo doped CaFeO3 electrode material for the application in supercapacitor. *Appl. Phys. A.* **131**, 382. https://doi.org/10.1007/s00339-025-08501-2 (2025).
14. Blaha, P., Schwarz, K., Madsen, G. K. H. & Kvasnicka, D. An augmented plane wave plus local orbitals program for calculating crystal properties, WIEN2k (2001).
15. Burke, K., Perdew, J. P. & Ernzerhof, M. Why semilocal functionals work: accuracy of the on-top pair density and importance of system averaging. *J. Chem. Phys.* **109** (10), 3760–3771 (1998).
16. Becke, A. D. & Johnson, E. R. A simple effective potential for exchange. *J. Chem. Phys.* **124**, 221101. https://doi.org/10.1063/1.2213970 (2006).
17. Tsuyama, T. et al. X-ray spectroscopic study of BaFeO3 thin films: an Fe4+ ferromagnetic insulator. *Phys. Rev. B.* **91**, 115101. https://doi.org/10.1103/PhysRevB.91.115101 (2015).
18. Chakraverty, S. et al. BaFeO3 cubic single crystalline thin film: A ferromagnetic insulator. *Appl. Phys. Lett.* **103**, 142416. https://doi.org/10.1063/1.4824210 (2013).
19. Hoedl, M. F., Ertural, C., Merkle, R., Dronskowski, R. & Maier, J. The orbital nature of electron holes in BaFeO3 and implications for defect chemistry. *J. Phys. Chem. C.* **126** (30), 12809–12819. https://doi.org/10.1021/acs.jpcc.2c02545 (2022).
20. Bouferrache, K. et al. Thermal, optoelectronic and thermoelectric properties of inorganic double perovskites semiconductors Cs2(Sn, Pt, Te)I6 for application as intermediate-band solar cells. *Solid State Commun.* **389**, 115522. https://doi.org/10.1016/j.ssc.2024.115522 (2024).
21. Ali, Z. et al. Theoretical studies of structural and magnetic properties of cubic perovskites PrCoO3 and NdCoO3. *Phys. B.* **406** (20), 3800–3804 (2011).
22. Ghebouli, M. A., Bouferrache, K., Alanazi, F. K., Ghebouli, B. & Fatmi, M. Stability, mechanical, optoelectronic and thermoelectric behaviors of inorganic metal halide double perovskites (Cs2, K2, Rb2)SnCl6: promising green energy alternatives. *Solid State Commun.* **397**, 115831. https://doi.org/10.1016/j.ssc.2025.115831 (2025).
23. Asfora, A. N., Haid, S. & Ould Moussa, M. A comprehensive numerical investigation on structural stability, mechanical, and optoelectronic properties of HfxSi1-xO2 tetragonal compounds from the Hafnon family. *Comput. Theor. Chem.* **1241**, 114894. https://doi.org/10.1016/j.comptc.2024.114894 (2024).
24. Ould Moussa, M. et al. Theoretical investigation on the optoelectronic properties of ZrxSi1-xO2 tetragonal hypothetical alloys from Zircon family. *Appl. Phys. A.* **128**, 231. https://doi.org/10.1007/s00339-022-05362-x (2022).
25. Haid, S. et al. Investigation of DFT+U effect of holmium rare-earth on the electronic, magnetic and the half-metallic ferromagnetic properties' of double perovskite Ba2HoReO6. *Solid State Commun.* **294**, 29–35. https://doi.org/10.1016/j.ssc.2019.03.001 (2019).
26. Haid, S. et al. Numerical assessment of physical properties of Ba2DyTaO6 ferroelectric rare Earth-Based compound and Estimation of the curie temperature for energy harvesting and spintronic applications. *J. Electron. Mater.* **53**, 75–85. https://doi.org/10.1007/s11664-023-10747-6 (2024).
27. Mir, S. A. & Gupta, D. C. New ferromagnetic half-metallic perovskites for spintronic applications: BaMO3 (M = Mg and Ca). *RSC Adv.* **10**, 26277 (2020).
28. KaleemullahN.S., HussainM.S., Ashwin, V., Ajay, G. & SirajuddeenM.M.S. Novel ternary halide perovskite AMX3 (A/M = Li, Na, K, Rb, Be, Mg, Ca, Sr, Ba, X = Br, Cl, F, I) for optoelectronic applications. *Chem. Phys. Impact*. **8**, 100545. https://doi.org/10.1016/j.chphi.2024.100545 (2024).
29. Sirajuddeen, M. M. S. & Banu, I. B. S. Electronic and magnetic properties of Fe(Mn)-doped cd and Zn nitrides for spintronic applications: a first-principles study. *J. Mater. Sci.* **50**, 1446–1456. https://doi.org/10.1007/s10853-014-8705-2 (2015).
30. Sirajuddeen, M. M. S. et al. A DFT+U study to report magnetic phase transition, electronic properties and half metallic ferromagnetism in palladium oxide using Hubbard method. *Mater. Chem. Phys.* **241**, 122263. https://doi.org/10.1016/j.matchemphys.2019.122263 (2020).
31. Ghebouli, M. A., Bouferrache, K., Alanazi, F. K., Ghebouli, B. & Fatmi, M. Computational insights into the Stability, Mechanical, optoelectronic, and thermoelectric characteristics investigation on Lead-Based double perovskites of (Cs2, K2, Rb2)PbCl6: promising candidates for optoelectronic applications. *Adv. Theory Simul.* 2400938. https://doi.org/10.1002/adts.202400938 (2024).

32. Batool, A., Saleem, M. I., Zhu, Y., Ma, X. & Cao, C. First-principles calculations of electronic, optical and thermodynamic properties of MTe (M=Ge, Sn): Spin-induced modulations in electronic and optical properties. *Comput. Mater. Sci.* **254**, 113907 (2025).
33. Bouferrache, K. et al. The impact of functionals on BiGaO3 structural, electronic, optical and thermoelectric properties. *Chem. Phys. Impact*. **5**, 100110. https://doi.org/10.1016/j.chphi.2022.100110 (2022).

Acknowledgements
The authors extend their appreciation to Taif University, Saudi Arabia, for supporting this work through project number (TU-DSPP-2024-63).

Author contributions
Authors StatementsConceptualization: K. BouferracheData curation: M.A. Ghebouli, Mohamed (A) Habila Analysis : (B) Ghebouli, S. AlomairyValidation : Faisal Katib Alanazi, M. Fatmi.

Declarations

Competing interests
The authors declare no competing interests.

Additional information
Correspondence and requests for materials should be addressed to M.F.

Reprints and permissions information is available at www.nature.com/reprints.

Publisher's note Springer Nature remains neutral with regard to jurisdictional claims in published maps and institutional affiliations.